

Anomalous Decay Rate and Greybody Factors for Regular Black Holes with Scalar Hair

Ramón Bécar,^{1,*} P. A. González,^{2,†} Eleftherios Papantonopoulos,^{3,‡} and Yerko Vásquez^{4,§}

¹*Departamento de Ciencias Matemáticas y Físicas, Facultad de Ingeniería, Universidad Católica de Temuco, Montt 56, Casilla 15-D, Temuco, Chile.*

²*Facultad de Ingeniería y Ciencias, Universidad Diego Portales, Avenida Ejército Libertador 441, Casilla 298-V, Santiago, Chile.*

³*Physics Division, School of Applied Mathematical and Physical Sciences, National Technical University of Athens, 15780 Zografou Campus, Athens, Greece.*

⁴*Departamento de Física, Facultad de Ciencias, Universidad de La Serena, Avenida Cisternas 1200, La Serena, Chile.*

We study the propagation of massive scalar fields in the background of asymptotically flat regular black holes supported by a phantom scalar field with a scalar charge A . This parameter regularizes the geometry by removing the central singularity. Focusing on wave dynamics, we analyze scalar perturbations, quasinormal modes, and greybody factors, emphasizing the role of the regularization parameter on the effective potential and the decay properties of the modes. Using WKB methods beyond the eikonal limit, we show that the presence of scalar hair modifies both the oscillation frequencies and damping rates of quasinormal modes. In particular, we demonstrate the occurrence of an anomalous decay rate for massive scalar perturbations, and above a critical field mass, the longest-lived modes correspond to lower angular momentum, in contrast with the massless case. We derive analytical expressions for the critical mass and study its dependence on the scalar charge and overtone number. Furthermore, we apply the Horowitz–Hubeny method to compute the quasinormal frequencies and show that the results obtained from the WKB and Horowitz–Hubeny approaches exhibit excellent agreement in the regime where both methods are valid. In addition, we compute reflection and transmission coefficients and analyze the corresponding greybody factors, clarifying how regularity effects imprint themselves on black-hole scattering properties. Our results show that regular black holes with scalar hair exhibit distinctive dynamical signatures that can be probed through quasinormal ringing and wave propagation.

PACS numbers:

Contents

I. Introduction	1
II. Setup of the theory of Regular black holes	3
III. Scalar field perturbations	5
IV. Photon Sphere Modes	5
A. WKB approximation	5
B. Horowitz–Hubeny method	9
V. Greybody Factors	11
VI. Conclusions	13
A. Full third-order WKB expressions for the QNFs and critical mass	13
B. Near-horizon series expansions	14

Acknowledgments

16

References

16

I. INTRODUCTION

The creation of matter at the end of inflation in standard cosmology allows the Universe to enter a deceleration regime and then to return to an accelerated phase again. The recent observational results indicate that the cosmological evolution at early time, the matter structure formation of the Universe was governed by a peculiar matter, the dark matter. Dark matter is a mysterious form of matter. Its properties and characteristics remain largely unknown. Nevertheless, astronomical observations indicate that dark matter accounts for more than 30% of the total matter–energy content of the Universe. Dark energy is a peculiar form of energy and may point to still unknown forms of matter–energy in the Universe [1]. The dark energy which was characterized by negative values of the pressure to density ratio w which could even be $w < -1$ [2–7]. The negative value of $w < -1$ imposes a constraint on the nature of dark energy and should be parametrized by a *phantom field* having negative kinetic energy [8–10]. However, in this case, a perfect-fluid description of dark energy described by an imaginary veloc-

*Electronic address: rbecar@uct.cl

†Electronic address: pablo.gonzalez@udp.cl

‡Electronic address: lpapa@central.ntua.gr

§Electronic address: yvasquez@userena.cl

ity of sound that characterizes the phantom-matter case is plagued with instabilities at small scales. To avoid this instability, a phantom scalar field may be regarded as an effective field description following from an underlying theory with positive energies [11, 12].

If dark matter can undergo gravitational condensation, star-like objects composed of dark matter may be created in the Universe. Such dark matter objects could be optically transparent, providing a possible explanation for the central bright spot observed in the Universe. In the same time, the problem of black hole (BH) singularities is a central issue in theoretical physics. It is well known that the cosmic censorship conjecture postulates that singularities are covered by an one-way event horizon. In 1968, Bardeen [13] proposed a novel approach by constructing a BH metric in which the central singularity is removed; such objects are known as regular BHs. Recently, it was claimed that BHs can be supported by astrophysical and cosmological observations as realistic astrophysical BH models [14]. In this way non-singular cosmological BH models can couple to the expansion of the Universe, gaining mass proportional to the scale factor. This claim was based on a recent study of supermassive BHs within elliptical galaxies [15]. This leads to a realistic behavior at infinity of BH models predicting that the gravitating mass of a BH can increase with the expansion of the Universe in a manner that depends on the BH interior solution. Then in [14] it was proposed that stellar remnant BHs are the astrophysical origin of dark energy, explaining the onset of accelerating expansion of the Universe.

A gravity theory with a scalar field minimally coupled to gravity with arbitrary potentials and negative kinetic energy was investigated in [16] and local solutions were produced. It was found that regular configurations were formed by the phantom scalar field in flat, de Sitter (dS) and anti-de Sitter (AdS) asymptotic spacetimes, avoiding the BH central singularity. The motivation of these studies was to find regular BH solutions with an expanding, asymptotically de Sitter Kantowski-Sachs cosmology beyond the event horizon. These geometries corresponds to what are known as black universes. Alternative solutions with a regular center have also been reported in the literature [17–19].

A gravitational model in the presence of a self-interacting phantom scalar field with a scalar charge A , minimally coupled to gravity was studied in [20]. If the scalar charge is zero, then the gravitational singularity is covered by a horizon, and then a normal BH with a constant scalar field is found. However, if A is not zero, then the scalar charge of the phantom scalar field deforms the geometry in such a way that the gravitational singularity is absent and a compact object is generated with a horizon, which is a regular BH. It was found that the charge of the scalar field is connected to the mass of the BH dressing in this way the BH with secondary hair.

Quasinormal modes (QNMs) provide a direct link between the perturbative dynamics of compact objects and

gravitational-wave observations [21–23]. In particular, the ringdown phase of a binary merger is governed by a superposition of damped oscillations whose frequencies and decay rates are determined by the underlying spacetime geometry. Therefore, any modification of the effective potential, such as those arising in black-universe configurations [16], may lead to observable deviations in the quasinormal spectrum. The linear stability of these configurations was investigated in [24], where it was shown that stability is not a generic feature, but rather occurs only within a restricted region of parameter space. In particular, while most configurations are unstable under spherically symmetric perturbations, there exists a special subset of solutions—characterized by specific parameter relations—for which the system remains stable. Outside this regime, the effective potential typically develops negative gaps that can trigger unstable modes or significantly modify the damping times. Even within the stable sector, the modified global structure of these geometries—namely, the presence of a regular interior connected to an expanding region beyond the horizon—affects the shape of the effective potential and, consequently, the associated quasinormal spectrum.

From an observational perspective, these effects would manifest as shifts in the ringdown frequencies and decay rates relative to those predicted for standard black holes. Such deviations could, in principle, be probed through black hole spectroscopy with current and future gravitational-wave detectors [25–28]. However, a quantitative assessment of detectability requires embedding these solutions into realistic astrophysical scenarios and constructing full waveform templates [29–32].

When a black hole spacetime is perturbed by a massless scalar field, the longest-lived quasinormal modes are those with higher angular number ℓ . However, in the presence of a massive scalar field: above a certain critical value of the scalar field mass, the hierarchy of damping times is inverted, and the longest-lived modes become those with lower angular number. This inversion can be understood from the additional energy stored in the massive perturbation, which reshapes the subleading structure of the effective potential and modifies the decay pattern of the modes. The phenomenon is known to occur in asymptotically flat, asymptotically dS, and asymptotically AdS spacetimes; however, the existence of a critical mass has been established only for asymptotically flat and asymptotically dS geometries, as it does not arise for large or intermediate AdS black holes. The anomalous decay of quasinormal modes has been widely explored for scalar fields [33–43], for charged scalar perturbations [44, 45], and for fermionic fields [46]. The effect has also been analyzed in accelerating black holes [47], and more recently in wormhole geometries [48, 49], showing that it is a robust feature in a broad class of gravitational backgrounds.

In a recent study [50], following [16, 20] we considered a phantom scalar field with a scalar charge A in a four-dimensional gravity theory, and analyzed time-

like geodesic motion focusing on bound and unbound trajectories and on weak-field observables. In particular, we derived the perihelion precession of bound orbits and used Solar System data to constrain the parameter controlling the regularization of the geometry. These results provide an independent, observationally motivated characterization of the underlying spacetime and delimit the physically relevant region of the parameter space. In the present work, we complement that particle-dynamics perspective with a wave-dynamics analysis by studying the propagation of massive fields, quasinormal ringing, and transmission/reflection probabilities, thereby clarifying how the same regularizing parameter imprints itself both on orbital tests and on the dynamical response of the black hole.

The paper is organized as follows. In Sec. II, we present the theoretical setup of regular black holes and summarize the main properties of the corresponding spacetime geometry. Sec. III is devoted to the analysis of scalar field perturbations propagating on this background. In Sec. IV, we investigate the photon-sphere quasinormal modes and analyze the anomalous behavior of the decay rate of the modes. Sec. V focuses on the computation of greybody factors. Finally, Sec. VI contains our conclusions.

II. SETUP OF THE THEORY OF REGULAR BLACK HOLES

We consider the action

$$S = \int d^4x \sqrt{-g} \left[\frac{R}{2\kappa} - \frac{1}{2} f(\phi) \nabla_\mu \phi \nabla^\mu \phi - V(\phi) \right], \quad (1)$$

where R ¹ is the Ricci scalar, $\kappa = 8\pi G$ with $G = 1$, and ϕ is a self interacting scalar field. The function $f(\phi)$ determines the nature of the scalar field: canonical if $f > 0$, phantom if $f < 0$. The Einstein and scalar field equations are

$$G_{\mu\nu} = \kappa T_{\mu\nu}, \quad (2)$$

$$f(\phi) \square \phi + \frac{f'(\phi)}{2} \nabla_\mu \phi \nabla^\mu \phi = \frac{dV}{d\phi}, \quad (3)$$

with

$$T_{\mu\nu} = f(\phi) \nabla_\mu \phi \nabla_\nu \phi - \frac{f(\phi)}{2} g_{\mu\nu} \nabla_\alpha \phi \nabla^\alpha \phi - V(\phi). \quad (4)$$

We consider a static, spherically symmetric metric

$$ds^2 = -b(r) dt^2 + \frac{1}{b(r)} dr^2 + w(r)^2 d\Omega^2, \quad (5)$$

where

$$d\Omega^2 = d\theta^2 + \sin^2 \theta d\varphi^2, \quad (6)$$

and

$$w(r) = \sqrt{r^2 + A^2}, \quad (7)$$

where the parameter A is a length scale. In [16] a class of static, spherically symmetric regular black hole solutions with a phantom scalar field was constructed and the associated stress-energy tensor was analyzed, including the evaluation of the corresponding energy conditions.

For a phantom scalar field ($f(\phi) = -1$), one finds the following exact solution:

$$b(r) = c_1 (A^2 + r^2) - \frac{c_2 \left((A^2 + r^2) \tan^{-1} \left(\frac{r}{A} \right) + Ar \right) + 2Ar^2}{2A^3}, \quad (8)$$

and the scalar field and the potential reads

$$\phi(r) = \frac{1}{2\sqrt{\pi}} \tan^{-1} \left(\frac{r}{A} \right), \quad (9)$$

$$V(\phi) = \frac{4A (A^2 c_1 - 1) (\cos(4\sqrt{\pi}\phi) - 2)}{32\pi A^3} + \frac{c_2 (3 \sin(4\sqrt{\pi}\phi) - 4\sqrt{\pi}\phi (\cos(4\sqrt{\pi}\phi) - 2))}{32\pi A^3}. \quad (10)$$

The asymptotic expansion of the scalar field at spatial infinity yields

$$\phi(r \rightarrow \infty) = \frac{\sqrt{\pi}A}{4|A|} - \frac{1}{2\sqrt{\pi}} \frac{A}{r} + \mathcal{O} \left(\frac{A^3}{r^3} \right). \quad (11)$$

From this expression it follows that the parameter A determines the leading $1/r$ fall-off of the scalar field and therefore can be interpreted as a scalar charge.

The large- r expansion of the metric function yields

$$b(r \rightarrow \infty) \sim r^2 \left(c_1 - \frac{4A + \pi c_2}{4A^3} \right) + \left(A^2 c_1 - \frac{\pi c_2}{4A} \right) + \frac{c_2}{3r} - \frac{A^2 c_2}{15r^3} + \mathcal{O}(1/r^5). \quad (12)$$

In this form, the leading behavior of $b(r)$ resembles that of a Schwarzschild-(Anti)-de Sitter spacetime, with an effective cosmological term proportional to r^2 and sub-leading corrections that depend on the scalar charge A and the integration constants. To clarify the asymptotic structure, one can perform a coordinate redefinition $r^2 = R(r)^2 - A^2$, in terms of a new radial coordinate R , after which the expansion becomes

$$b(R \rightarrow \infty) \sim R^2 \left(-\frac{\pi c_2}{4A^3} - \frac{1}{A^2} + c_1 \right) + 1 + \frac{c_2}{3R} + \mathcal{O}(1/R^3). \quad (13)$$

In the above expansion there is no deficit angle at spatial infinity, indicating that the geometry does not correspond

¹ Our conventions and definitions throughout this paper are: $(-, +, +, +)$ for the signature of the metric, the Riemann tensor is defined as $R^\lambda{}_{\mu\nu\sigma} = \partial_\nu \Gamma^\lambda{}_{\mu\sigma} - \partial_\sigma \Gamma^\lambda{}_{\mu\nu} + \Gamma^\rho{}_{\mu\sigma} \Gamma^\lambda{}_{\rho\nu} - (\nu \leftrightarrow \sigma)$, and the Ricci tensor and scalar are given by $R_{\mu\nu} = R^\lambda{}_{\mu\lambda\nu}$ and $R = g^{\mu\nu} R_{\mu\nu}$ respectively.

to a global monopole but rather to a genuine black hole spacetime free of angular deficits.

To ensure that the spacetime is asymptotically flat, one can fix the integration constants by imposing

$$A^2 c_1 - \frac{\pi c_2}{4A} = 1 \rightarrow c_1 = \frac{4A + \pi c_2}{4A^3}. \quad (14)$$

With this choice, the asymptotic expansion of the metric function simplifies to

$$b(r) \sim 1 + \frac{c_2}{3r} - \frac{A^2 c_2}{15r^3} + \frac{A^4 c_2}{35r^5} + \mathcal{O}(1/r^7). \quad (15)$$

In this form, the spacetime is manifestly asymptotically flat, approaching Minkowski space at large r , and closely resembles the Schwarzschild solution up to corrections sourced by the phantom scalar charge A . For the present solution, the conserved mass can be computed using the Abbott-Deser prescription for asymptotically flat spacetimes:

$$m = \frac{1}{2} \lim_{r \rightarrow \infty} r \left(\frac{1}{b(r)} - 1 \right) = -\frac{c_2}{6}, \quad (16)$$

demonstrating that the scalar field does not directly contribute to the conserved mass. Consequently, the spacetime describes a regular, asymptotically flat black hole carrying a primary phantom scalar hair without altering the global mass of the system. Using $m = -c_2/6$, the scalar potential can be written as

$$V(\phi) = \frac{3m}{16\pi A^3} \left[-8\sqrt{\pi}\phi - 3\sin(4\sqrt{\pi}\phi) \right. \\ \left. + 2\pi - (\pi - 4\sqrt{\pi}\phi) \cos(4\sqrt{\pi}\phi) \right]. \quad (17)$$

The horizon is determined by the roots of $b(r) = 0$. However, this equation cannot be solved analytically in closed form. To understand the existence of a horizon, it is useful to examine the behavior of $b(r)$ near the origin

$$b(r \rightarrow 0) \sim \frac{4A - 6\pi m}{4A} + \frac{6mr}{A^2} - \frac{3(\pi m)r^2}{2A^3} + \mathcal{O}(r^3), \quad (18)$$

where the dominant contribution is the constant term $(4A - 6\pi m)/4A$. The sign of the leading constant term controls the existence of a finite root. For $r > 0$, the linear term is positive, so a zero requires $m > 2A/3\pi$. Conversely, for $r < 0$ the linear term is negative, yielding a finite negative root only if $m < 2A/3\pi$. At the critical value $m = 2A/3\pi$, the constant term vanishes and the horizon is located at $r = 0$, coinciding with the minimum of the area function $w(r)$. The linear stability of these configurations under spherically symmetric perturbations was analyzed in [24]. Although most configurations are unstable under radial perturbations, a restricted subset of solutions satisfying specific parameter relations remains stable. This occurs precisely when the event

horizon coincides with the minimum of the areal radius, that is $m = 2A/3\pi$.

Asymptotically flat black hole. Let us consider the asymptotically flat solution, $c_1 = \frac{1}{A^2} - \frac{3\pi m}{2A^3}$, $c_2 = -6m$ and $A \leq \frac{3\pi m}{2}$. The lapse function $b(r)$ is given by

$$b(r) \equiv \frac{3m}{A^2} r - \frac{r^2}{A^2} + \frac{(4A - 6\pi m)(r^2 + A^2)}{4A^3} + \\ + \frac{3m(r^2 + A^2)}{A^3} \arctan \frac{r}{A}. \quad (19)$$

Fig. 1 shows the radial profile of the lapse function $b(r)$ for different values of the parameter A . In the Schwarzschild limit ($A = 0$), the lapse vanishes at the horizon, recovering the standard black hole solution. However, for $A > 0$, the family of solutions corresponds to regular black holes, where the central singularity is removed while maintaining asymptotic flatness. Increasing values of A shift the position of the event horizon toward smaller values of the radial coordinate r . However, the invariant areal radius of the horizon, $w(r_+)$, actually increases with A . At the same time, the spacetime smoothly approaches the flat limit at large distances. At the critical value $A \simeq 4.71$, the lapse vanishes only at the limit $r_+ = 0$, at which point the horizon matches the minimum of the area function.

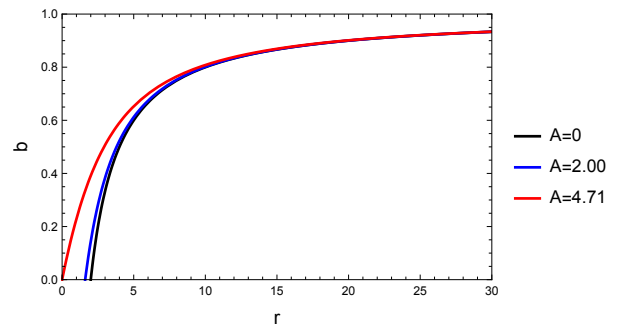


FIG. 1: Plot of the lapse function $b(r)$. Here we have used the value $m = 1$. The event horizon is at $r_+ = 2.000$ for $A = 0$, $r_+ = 1.610$ for $A = 2.00$, and $r_+ = 0$ for $A = 4.71$.

As we discussed in this section, the parameter A is a phantom scalar hair and when the scalar field backreacts to the metric, A becomes a primary scalar charge. Above all, the most important role of this parameter is that it makes the black hole regular.

Note, however, that the mass parameter m , which arises as an integration constant, appears explicitly in the scalar potential (17), i.e. in a quantity that defines the theory itself. Consequently, varying the black hole mass would effectively modify the underlying theory rather than simply selecting a different solution within the same model. Therefore, we introduce the constant $c = m/A^3$, which is treated as the parameter entering the scalar potential. With this redefinition, the mass parameter is no longer independent of the scalar charge A , and

the scalar hair becomes secondary, i.e., it is determined by the black hole parameters rather than introducing an additional independent charge. With this parameterization, the scalar potential no longer depends on the scalar charge:

$$V(\phi) = \frac{3c}{16\pi} \left[-8\sqrt{\pi}\phi - 3\sin(4\sqrt{\pi}\phi) + 2\pi - (\pi - 4\sqrt{\pi}\phi) \cos(4\sqrt{\pi}\phi) \right], \quad (20)$$

and the metric function can be written as

$$b(r) = 3cAr - \frac{r^2}{A^2} + \frac{(4 - 6\pi cA^2)(r^2 + A^2)}{4A^2} + 3c(r^2 + A^2) \arctan \frac{r}{A}. \quad (21)$$

Expanding $b(r)$ for small A/r yields

$$b(r) \approx 1 - \frac{2cA^3}{r} + \frac{2cA^5}{5r^3} + \mathcal{O}(A^7) \quad (22)$$

and in the limit $A = 0$ the metric reduces to Minkowski spacetime. With this parameterization, the event horizon coincides with the minimum of the areal radius for $c = 2/(3\pi A^2)$. In the following, we study how this parameter influences the QNMs and greybody factors.

III. SCALAR FIELD PERTURBATIONS

The QNMs of scalar perturbations in the background of the metric (5) for the asymptotically flat black hole defined by $b(r)$ in (21), are determined by solving the Klein-Gordon equation for a scalar field in this spacetime

$$\frac{1}{\sqrt{-g}} \partial_\mu (\sqrt{-g} g^{\mu\nu} \partial_\nu \varphi) = \bar{m}^2 \varphi, \quad (23)$$

with suitable boundary conditions for a black hole geometry. In the above expression \bar{m} is the mass of the scalar field φ . Now, by means of the following ansatz

$$\varphi = e^{-i\omega t} R(r) Y(\Omega), \quad (24)$$

the Klein-Gordon equation reduces to

$$b(r) \partial_r^2 R(r) + \left(\frac{2w'(r)b(r)}{w(r)} + b'(r) \right) \partial_r R(r) + \left(\frac{\omega^2}{b(r)} + \frac{\kappa}{w^2(r)} - \bar{m}^2 \right) R(r) = 0, \quad (25)$$

where we defined $\kappa = -\ell(\ell + 1)$, with $\ell = 0, 1, 2, \dots$, which represents the eigenvalue of the Laplacian on the two-sphere and ℓ is the multipole number. Now, by using the tortoise coordinate r^* given by $dr^* = \frac{dr}{b(r)}$, and then

defining $R(r) = \frac{F(r)}{w(r)}$ the Klein-Gordon equation can be written as an one-dimensional Schrödinger-like equation

$$\frac{d^2 F(r^*)}{dr^{*2}} - V_{\text{eff}}(r) F(r^*) = -\omega^2 F(r^*), \quad (26)$$

with an effective potential $V_{\text{eff}}(r)$, which parametrically thought, $V_{\text{eff}}(r^*)$, is given by

$$V_{\text{eff}}(r) = b(r) \left(\bar{m}^2 - \frac{\kappa}{w(r)^2} + \frac{(b(r)w'(r))'}{w(r)} \right). \quad (27)$$

Fig. 2 presents the effective potential $V_{\text{eff}}(r)$ for a massive scalar field ($\bar{m} = 0.1$) and different values of the deformation parameter A . The potential displaying a single peak that governs the propagation and trapping of scalar perturbations. As A increases, both the height and width of the potential barrier decrease and its maximum shifts slightly toward larger radii. This behavior indicates that the deformation weakens the near-horizon confinement and displaces the dominant interaction region outward, while the spacetime remains asymptotically flat.

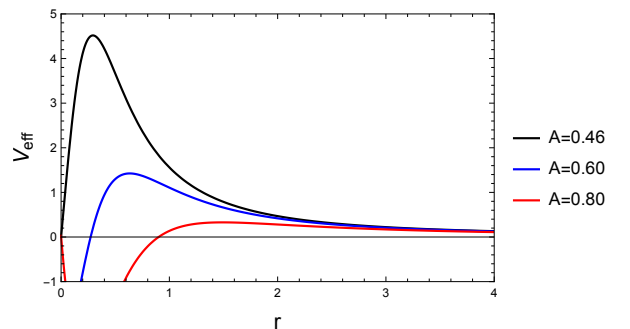


FIG. 2: Plot of the effective potential as a function of r . Here, we have used the value $c = 1$, $\bar{m} = 0.1$ and $\ell = 1$. The event horizon is at $r_+ = 0$ for $A = 0.46$, $r_+ = 0.273$ for $A = 0.60$, and $r_+ = 0.901$ for $A = 0.80$.

IV. PHOTON SPHERE MODES

In this section, we use the WKB approximation and the Horowitz–Hubeny method to compute the quasinormal frequencies (QNFs) associated with photon-sphere modes.

A. WKB approximation

In this section, we employ the WKB approximation method, originally proposed by Mashhoon [52] and subsequently developed by Schutz and Iyer [53]. The third-order formulation introduced by Iyer and Will [54] was later extended to sixth order [55], and more recently

to thirteenth order [56]; see also [57] for a comprehensive overview. This semi-analytic technique has been successfully applied to compute QNFs of both asymptotically flat and asymptotically de Sitter black holes. The WKB method is particularly well suited for effective potentials of barrier type, whose asymptotic behavior approaches constant values at the horizon and at spatial infinity [23]. However, it should be emphasized that this method captures only the modes associated with the photon sphere. The QNMs are determined by the behavior of the effective potential in the vicinity of its maximum $V(r_{max}^*)$, around which the potential can be expanded in a Taylor series of the form

$$V(r^*) = V(r_{max}^*) + \sum_{k=2}^{k=\infty} \frac{V^{(k)}}{k!} (r^* - r_{max}^*)^k, \quad (28)$$

where

$$V^{(k)} = \frac{d^k}{dr^{*k}} V(r^*)|_{r^*=r_{max}^*}, \quad (29)$$

corresponds to the k -th derivative of the potential with respect to r^* , evaluated at the position of the maximum of the potential, r_{max}^* . Using the WKB approximation up to third order beyond the eikonal limit, the QNFs are given by the following expression [54, 58]

$$\omega^2 = V(r_{max}^*) - 2iU, \quad (30)$$

where

$$U = N\sqrt{-V^{(2)}/2} + \frac{i}{64} \left[-\frac{1}{9} \frac{V^{(3)2}}{V^{(2)2}} (7 + 60N^2) + \frac{V^{(4)}}{V^{(2)}} (1 + 4N^2) \right] + \frac{N}{2^{3/2}288} \left[\frac{5}{24} \frac{V^{(3)4}}{(-V^{(2)})^{9/2}} (77 + 188N^2) + \frac{3}{4} \frac{V^{(3)2}V^{(4)}}{(-V^{(2)})^{7/2}} (51 + 100N^2) + \frac{1}{8} \frac{V^{(4)2}}{(-V^{(2)})^{5/2}} (67 + 68N^2) + \frac{V^{(3)}V^{(5)}}{(-V^{(2)})^{5/2}} (19 + 28N^2) + \frac{V^{(6)}}{(-V^{(2)})^{3/2}} (5 + 4N^2) \right],$$

and $N = n + 1/2$, with $n = 0, 1, 2, \dots$, is the overtone number.

Defining $L^2 = \ell(\ell + 1)$, we find that for large values of L , the maximum of the potential is approximately at

$$r_{max} \approx r_0 + \frac{r_1}{L^2}, \quad (31)$$

where

$$r_0 = 3cA^3, \quad (32)$$

$$r_1 = \frac{3}{2}cA^3\xi\eta \left[-27\pi A^6 c^3 + 18A^4 c^2 - 3\pi A^2 c + 1 + A^2 \xi (6c \arctan(3A^2 c) + \bar{m}^2) \right], \quad (33)$$

with $\eta = 2 - 3\pi cA^2 + 6cA^2 \arctan(3cA^2)$, and $\xi = 1 + 9c^2 A^4$. So, the maximum of the potential is

$$V(r_{max}^*) \approx V_0 L^2 + V_1, \quad (34)$$

where

$$V_0 = \frac{\eta}{2A^2}, \quad (35)$$

$$V_1 = \frac{\eta}{4A^2} \left[2\bar{m}^2 A^2 \xi + (1 + 18c^2 A^4) \eta \right], \quad (36)$$

while the higher order derivatives $V^{(k)}(r_{max}^*)$ for $k = 2, \dots, 6$, can be expressed in the following abbreviated manner

$$V^{(2)}(r_{max}^*) \approx V_0^{(2)} L^2 + V_1^{(2)}, \quad (37)$$

$$V^{(3)}(r_{max}^*) \approx V_0^{(3)} L^2, \quad (38)$$

$$V^{(4)}(r_{max}^*) \approx V_0^{(4)} L^2, \quad (39)$$

$$V^{(5)}(r_{max}^*) \approx V_0^{(5)} L^2, \quad (40)$$

$$V^{(6)}(r_{max}^*) \approx V_0^{(6)} L^2. \quad (41)$$

where

$$V_0^{(2)} = -\frac{\eta^2}{2A^4}, \quad (42)$$

$$V_1^{(2)} = -\frac{\eta^2}{4A^4} \left[\eta \left(1215\pi A^{10} c^5 - 810A^8 c^4 + 162\pi A^6 c^3 - 54A^4 c^2 + 3\pi A^2 c + 2 + (-2430A^{10} c^5 - 324A^6 c^3 - 6A^2 c) \arctan(3A^2 c) \right) + 3cA^4 \bar{m}^2 \xi \times \left(15A^2 c (3\pi A^2 c - 2) - 2(45A^4 c^2 + 1) \arctan(3A^2 c) + \pi \right) \right], \quad (43)$$

$$V_0^{(3)} = \frac{3c\eta^3}{2A^3}, \quad (44)$$

$$V_0^{(4)} = \frac{3(2 - \pi cA^2 + 2cA^2 \arctan(3cA^2))\eta^3}{2A^6}, \quad (45)$$

$$V_0^{(5)} = -\frac{3c\eta^4(-3\pi cA^2 + 17 + 6cA^2 \arctan(3cA^2))}{2A^5}. \quad (46)$$

$$V_0^{(6)} = -\frac{9\eta^4}{2A^8} \left[A^2 c (A^2 c (45\pi A^2 c + \pi^2 - 30) - 10\pi) + 2A^2 c \arctan(3A^2 c) (-45A^4 c^2 - 2\pi A^2 c + 2A^2 c \arctan(3A^2 c) + 10) + 10 \right]. \quad (47)$$

Moreover, our interest is to evaluate the QNFs for large values of L , so we expand the frequencies as power series in L . It is important to keep in mind that in the eikonal limit, the leading term is linear in L . Next, we consider the following expression in powers of L

$$\omega = \omega_{1m}L + \omega_0 + \omega_1L^{-1} + \omega_2L^{-2} + \mathcal{O}(L^{-3}), \quad (48)$$

where

$$\omega_{1m} = \frac{1}{3\sqrt{3}A^3c} - \frac{1}{90\sqrt{3}A^7c^3} + \frac{79}{113400\sqrt{3}A^{11}c^5} + \dots,$$

$$\omega_0 = -\frac{i(2n+1)}{6\sqrt{3}A^3c} + \frac{i(2n+1)}{180\sqrt{3}A^7c^3} - \frac{79i(2n+1)}{226800\sqrt{3}A^{11}c^5} + \dots,$$

$$\omega_1 = \frac{1}{2}\sqrt{3}A^3c\bar{m}^2 + \frac{7\bar{m}^2}{60\sqrt{3}Ac} + \frac{17 - 15n(n+1)}{324\sqrt{3}A^3c} + \dots,$$

$$\omega_2 = \frac{5iA^3c\bar{m}^2(2n+1)}{4\sqrt{3}} - \frac{i(2n+1)(235n(n+1) + 137)}{23328\sqrt{3}A^3c} + \frac{i\bar{m}^2(2n+1)}{24\sqrt{3}Ac} + \dots,$$

by performing a series expansion in A/r_+ . The ellipsis denote terms of higher order in A/r_+ . In Appendix A, we show the full expression obtained without approximations.

The term proportional to $1/L^2$ in Eq. (48) vanishes at the value of the critical mass \bar{m}_c , which is given by

$$\bar{m}_c = \frac{1}{A^3c} \sqrt{\frac{137 + 235n(n+1)}{29160}} + \frac{151 - 235n(n+1)}{1620A^7c^3\sqrt{10(137 + 235n(n+1))}} + \dots \quad (49)$$

The first term in the expansion resembles the critical scalar field mass of the Schwarzschild case reported in [39]. The scalar charge A decreases the critical mass. The full expression for the critical mass is given in the appendix A. Fig. 3 shows the dependence of the critical mass \bar{m}_c on the deformation parameter A for the overtone numbers $n = 0, 1, 2$. The critical mass shows a monotonically decrease as the parameter A increases for all values of n , and tends to zero for high values of A , in agreement with (49). Furthermore, for any fixed value of A , the critical mass is an increasing function of the overtone number n .

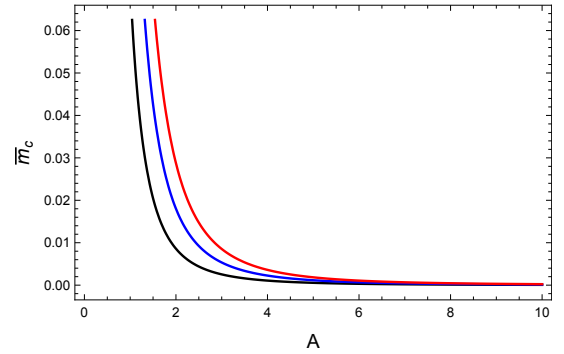


FIG. 3: The behavior of \bar{m}_c as a function of A for the overtone number $n = 0$ (black curve), $n = 1$ (blue curve) and $n = 2$ (red curve) with $c = 1$.

Now, to illustrate the anomalous behavior, we plot in Fig. 4 the behavior of $-Im(\omega)$ as a function of \bar{m} , using the 6th-order WKB method with Padé approximants. We observe an anomalous decay rate: $\bar{m} < \bar{m}_c$, the longest-lived modes correspond to the highest angular number ℓ , while for $\bar{m} > \bar{m}_c$, the longest-lived modes correspond to the lowest angular number.

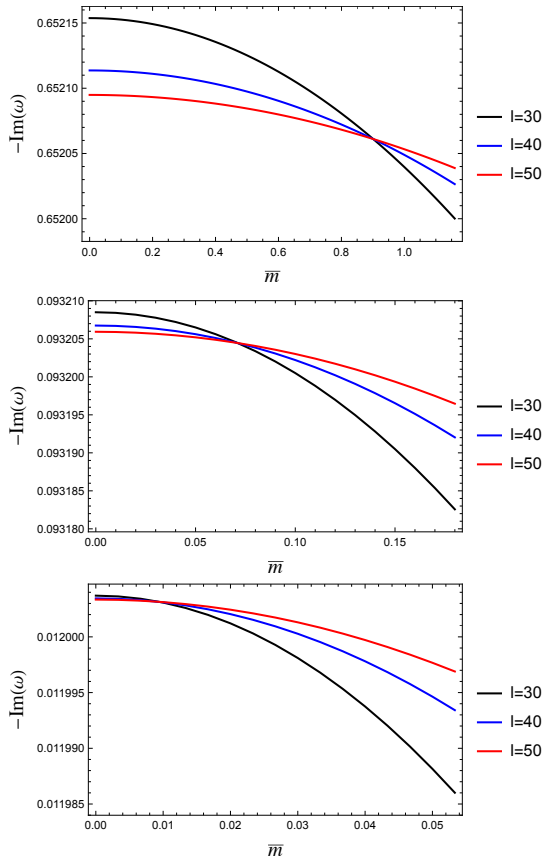


FIG. 4: The behavior of $-\text{Im}(\omega)$ for the fundamental mode ($n = 0$) as a function of the scalar field mass \bar{m} for different values of the angular number $\ell = 30$ (black curve), $\ell = 40$ (blue curve), $\ell = 50$ (red curve), with $c = 1$, $A = 0.4606$ (top panel), $A = 1$ (central panel), and $A = 2$ (bottom panel) using the 6th order WKB method with Padé approximants. Here, the WKB method yields critical masses of $\bar{m}_c \approx 0.901$, 0.071 and 0.009 , respectively, via Eq. (A5).

The behavior shown in Fig. 5 highlights an important contrast between the real and imaginary parts of the quasinormal spectrum. While the imaginary part exhibits a pronounced sensitivity to the scalar field mass, leading to the anomalous decay-rate phenomenon discussed previously, the real part of the frequency remains largely insensitive to \bar{m} . This indicates that the oscillation timescale of the perturbations is predominantly controlled by the geometry near the photon sphere, rather than by the mass of the scalar field.

Moreover, the monotonic decrease of $\text{Re}(\omega)$ with increasing scalar charge A reflects the weakening of the effective potential barrier induced by the regularizing parameter. As A increases, the height of the potential maximum decreases and its location is shifted outward, leading to lower characteristic oscillation frequencies. Nevertheless, the qualitative structure of the spectrum is preserved: the hierarchy in ℓ remains unchanged and no inversion analogous to the anomalous behavior observed

in the damping rates occurs.

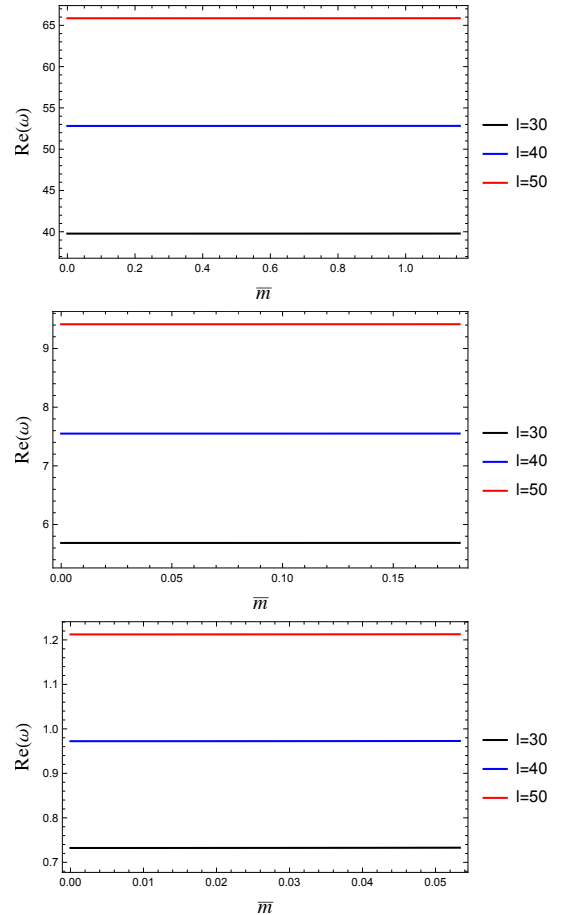


FIG. 5: The behavior of $\text{Re}(\omega)$ for the fundamental mode ($n = 0$) as a function of the scalar field mass \bar{m} for different values of the angular number $\ell = 30$ (black curve), $\ell = 40$ (blue curve), $\ell = 50$ (red curve), with $c = 1$, $A = 0.4606$ (top panel), $A = 1$ (central panel), and $A = 2$ (bottom panel) using the 6th order WKB method with Padé approximants.

The origin of the anomalous decay rate can be understood within the WKB framework by expressing the quasinormal spectrum in terms of the effective width of the potential barrier. The QNMs are determined by the behavior of the effective potential near its maximum, where the WKB condition relates the complex frequency to local properties of the barrier.

Rather than parameterizing the barrier in terms of its curvature, it is convenient to characterize it by its width Δr^* , which measures the extent of the classically forbidden region around the peak. Physically, Δr^* controls the trapping efficiency of the potential: wider barriers suppress tunneling and lead to longer-lived modes, whereas narrower barriers enhance leakage and increase the decay rate.

For massive scalar fields, the mass term modifies both the asymptotic structure and the shape of the effective potential, thereby altering the width of the barrier and

the system's ability to store energy. For sufficiently small field masses, increasing the multipole number ℓ broadens the effective barrier (larger Δr^*), enlarging the trapping region and suppressing tunneling. This results in longer-lived modes and gives rise to the anomalous decay behavior. In contrast, above a critical mass scale, the structure of the potential changes such that the barrier effectively narrows as ℓ increases. This reduces Δr^* , enhances tunneling, and leads to faster decay. In this picture, the anomalous decay rate reflects a transition in the effective width of the potential barrier.

To make this relation explicit, we define the width of the effective potential as the interval over which the potential decreases from its maximum value $V(r_{\max}^*)$ to a fraction ϵV . Expanding the potential to quadratic order around the maximum, one obtains

$$\Delta r^* \approx \sqrt{2(1-\epsilon) \frac{V(r_{\max}^*)}{-V^{(2)}(r_{\max}^*)}}. \quad (50)$$

Using the WKB expression for the QNFs, where the imaginary part is controlled by the second derivative of the potential at the peak, one finds

$$Im(\omega) \approx -\frac{1}{2\sqrt{2}} \sqrt{\frac{-V^{(2)}(r_{\max}^*)}{V(r_{\max}^*)}} + \mathcal{O}(1/L^2). \quad (51)$$

Substituting the above definition of the width, this can be rewritten as

$$Im(\omega) \approx -\frac{1}{2} \frac{\sqrt{1-\epsilon}}{\Delta r^*} + \mathcal{O}(1/L^2), \quad (52)$$

showing explicitly that, in the eikonal limit, the decay rate is inversely proportional to the width of the effective potential barrier [39, 43].

In Fig. 6 we plot the rescaled width $\Delta r^*/\sqrt{2(1-\epsilon)}$ as a function of the scalar field mass for different values of the multipole number. For masses below a given threshold, the width increases with ℓ , whereas for larger masses this behavior is reversed. Although this inversion does not occur exactly at the critical mass, it closely tracks the qualitative change observed in $Im(\omega)$, confirming that the anomalous decay is directly tied to the transition in the effective width of the potential barrier.

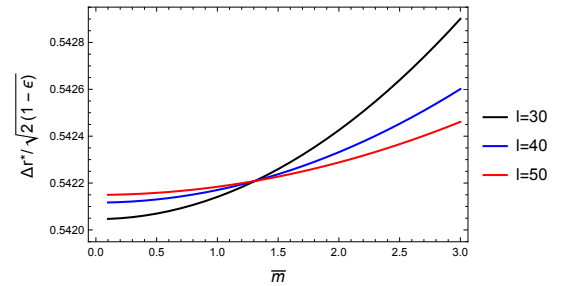


FIG. 6: Effective width of the potential barrier, $\Delta r^*/\sqrt{2(1-\epsilon)}$, as a function of the scalar field mass for different values of the multipole number $\ell = 30$ (black curve), $\ell = 40$ (blue curve), $\ell = 50$ (red curve), with $c = 1$ and $A = 0.4606$.

B. Horowitz–Hubeny method

Now, we apply a numerical procedure based on the Horowitz–Hubeny method (HHM) to compute the QNFs [59]. This method was originally developed for perturbations of asymptotically anti-de Sitter (AdS) black holes in the context of holography, where the quasinormal spectrum is related to the relaxation of perturbations in the dual field theory. It is particularly suitable for AdS spacetimes because the perturbation equation has regular singular points at the horizon and at infinity, allowing the solution to be constructed as a power series. The method consists of expanding the radial solution around the event horizon and imposing the boundary condition at spatial infinity, which selects a discrete set of complex frequencies corresponding to the QNMs. Here, we show that the standard HHM can also be applied to asymptotically flat black holes.

In this section we consider the approximation

$$A/r \ll 1, \quad r_+ < r < \infty, \quad (53)$$

which implies $A/r_+ \ll 1$. Under this assumption,

$$b(r) \approx 1 - \frac{2cA^3}{r}, \quad (54)$$

and $w(r)^2 = r^2 + A^2$. The event horizon is located at $r_+ \approx 2cA^3$, therefore

$$\frac{A}{r_+} = \frac{1}{2cA^2}, \quad (55)$$

so the approximation is valid in the regime $cA^2 \gg 1$.

To solve the radial equation (25), we impose the boundary conditions satisfied by the radial function $R(r)$. Near the horizon, only ingoing waves are allowed, so

$$R(r) \sim (r - r_+)^{-i\omega r_+} [1 + \mathcal{O}((r - r_+))]. \quad (56)$$

At spatial infinity, we impose outgoing-wave boundary conditions

$$R(r) \sim r^{-1 + \frac{ir_+(2\omega^2 - \bar{m}^2)}{2\sqrt{\omega^2 - \bar{m}^2}}} e^{i\sqrt{\omega^2 - \bar{m}^2}r} r \left[\frac{1}{r} + \mathcal{O}(1/r^2) \right]. \quad (57)$$

Note that a factor r has been deliberately kept outside the brackets to ensure that the quantity within the brackets vanishes as $r \rightarrow \infty$. Accordingly, we consider the ansatz

$$R(r) = (r - r_+)^{-i\omega r_+} r^{i\omega r_+ - 1 + \frac{ir_+(2\omega^2 - \bar{m}^2)}{2\sqrt{\omega^2 - \bar{m}^2}}} e^{i\sqrt{\omega^2 - \bar{m}^2}r} r \psi(r), \quad (58)$$

where the function $\psi(r)$ is regular at the horizon and decays as $1/r$ at spatial infinity, thereby satisfying the boundary condition $\psi(r) \rightarrow 0$ as $r \rightarrow \infty$ required by the standard HHM. Substituting this expression into the radial equation yields a differential equation for $\psi(r)$. We then introduce the compact coordinate $x = 1/r$, for which the horizon is mapped to $x_+ = 1/r_+$ and infinity to $x = 0$. The radial equation becomes

$$s(x)\psi''(x) + \frac{t(x)}{(x - x_+)}\psi'(x) + \frac{u(x)}{(x - x_+)^2}\psi(x) = 0, \quad (59)$$

where $s(x)$, $t(x)$, and $u(x)$ are fifth-degree polynomials (see Appendix B). The point $x = x_+$ is a regular singular point.

To compute the quasinormal frequencies, we expand the solution as a power series around the horizon

$$\psi(x) = (x - x_+)^a \sum_{n=0}^{\infty} a_n (x - x_+)^n. \quad (60)$$

From the indicial equation we obtain

$$a = 0, \quad a = 2i\omega/x_+. \quad (61)$$

The ingoing boundary condition selects $a = 0$. Truncating the series at order N and substituting into the radial equation yields the recurrence relation

$$a_n = -\frac{1}{P_n} \sum_{k=0}^{n-1} [k(k-1)s_{n-k} + kt_{n-k} + u_{n-k}] a_k, \quad (62)$$

with

$$\begin{aligned} P_n &= n(n-1)s_0 + nt_0 \\ &= 4nx_+(1 + x_+^2 A^2)(\omega^2 - \bar{m}^2)(nx_+ - 2i\omega). \end{aligned} \quad (63)$$

Since the equation has no poles in $0 < x < x_+$, the quasinormal mode condition is obtained by imposing the boundary condition $\psi(x) \rightarrow 0$ as $x \rightarrow 0$, which leads to the algebraic equation

$$\sum_{n=0}^N a_n (-x_+)^n = 0. \quad (64)$$

This condition is satisfied only for discrete complex values of ω , corresponding to the quasinormal spectrum.

To determine the zeros of the truncated series equation (64), we employ the Müller method [60], which is a three-point iterative root-finding algorithm particularly suitable for complex roots. The method generalizes the secant method by constructing a quadratic interpolating polynomial through three successive approximations of the function and taking one of its roots as the next iterate. Because it does not require derivatives and naturally handles complex numbers, it is well suited for quasinormal-mode calculations, where the frequency ω is complex. For sufficiently smooth functions and initial guesses close to the root, the method converges with order approximately 1.84, which is faster than the secant method and typically robust in complex root searches [61]. In practice, we evaluate the truncated series equation for complex values of ω and iterate until the relative change in the frequency satisfies the chosen numerical tolerance.

In Table I we present the QNFs of a massless scalar field obtained using the HHM and the sixth-order WKB approximation with Padé approximants for $c = 1$. The results are reported for several values of the multipole number ℓ , and for $A = 3$ and $A = 5$, considering the metric function (54). Furthermore, we show the relative error of the real and imaginary parts of the values obtained with the WKB method with respect to the values obtained with the HHM, which is defined by

$$\epsilon_{Re(\omega)} = \frac{|Re(\omega_{WKB}) - Re(\omega_{HHM})|}{|Re(\omega_{HHM})|} \cdot 100\%, \quad (65)$$

$$\epsilon_{Im(\omega)} = \frac{|Im(\omega_{WKB}) - Im(\omega_{HHM})|}{|Im(\omega_{HHM})|} \cdot 100\%. \quad (66)$$

We find excellent agreement between the two approaches within their common range of applicability. In particular, it is well known that the WKB approximation with Padé improvements yields reliable results when the multipole number ℓ is greater than the overtone number n , with the accuracy generally improving as ℓ increases relative to n ; for higher overtones with $n \gtrsim \ell$ the WKB results tend to lose precision.

The stability of the background geometry was analyzed in Ref. [24] within the linear approximation, where it was shown that these configurations are generically unstable under spherically symmetric perturbations, except for a special class of solutions in which the event horizon coincides with the minimum of the areal radius; the analysis includes both axial perturbations and the monopole sector of polar perturbations.

In the present work, we instead focus on the propagation of a test scalar field on these fixed backgrounds. Our analysis encompasses both the special class of configurations identified in Ref. [24] as stable, as well as cases in which the minimum of the areal function lies inside the horizon. Within this probe approximation, we find

TABLE I: The fundamental ($n = 0$) QNFs for several values of the angular momentum ℓ of a massless scalar field for the asymptotically flat regular black holes with $c = 1$, are calculated using the HHM and the sixth-order WKB method with Padé approximants. The QNFs obtained via the HHM have been calculated with nine decimal places of accuracy.

$A = 3$				
ℓ	HHM	WKB	$\epsilon_{Re(\omega)}(\%)$	$\epsilon_{Im(\omega)}(\%)$
0	0.004086511 - 0.003884059 i	0.004087112 - 0.003732616 i	0.015	3.9
1	0.010841490 - 0.003616272 i	0.010840493 - 0.003620066 i	0.009	0.105
2	0.017900157 - 0.003582881 i	0.017900083 - 0.003583152 i	0.0004	0.0076
3	0.024996222 - 0.0035732690 i	0.024996214 - 0.003573305 i	$3.2 \cdot 10^{-5}$	0.001
5	0.039217876 - 0.003567225 i	0.039217875 - 0.003567227 i	$2.5 \cdot 10^{-6}$	$5.6 \cdot 10^{-5}$
10	0.074812377 - 0.003564217 i	0.074812376 - 0.003564217 i	$1.3 \cdot 10^{-6}$	0
15	0.110419796 - 0.003563600 i	0.110419796 - 0.003563600 i	0	0
$A = 5$				
0	0.000883516 - 0.000839139 i	0.000883635 - 0.000806476 i	0.013	3.9
1	0.002343265 - 0.000781259 i	0.002343052 - 0.000782072 i	0.009	0.104
2	0.003868799 - 0.000774048 i	0.003868782 - 0.000774107 i	0.0004	0.0076
3	0.005402444 - 0.000771975 i	0.005402442 - 0.000771983 i	$3.7 \cdot 10^{-5}$	0.001
5	0.008476138 - 0.000770672 i	0.008476137 - 0.000770672 i	$1.2 \cdot 10^{-5}$	0
10	0.016169124 - 0.000770024 i	0.016169123 - 0.000770023 i	$6.2 \cdot 10^{-6}$	0.00013
15	0.023864910 - 0.000769890 i	0.023864909 - 0.000769890 i	$4.2 \cdot 10^{-6}$	0

no evidence of linear instabilities in the scalar sector for any configuration considered, including those that are unstable under gravitational perturbations. This indicates that, at the level of test-field dynamics, the spacetimes support well-defined quasinormal ringing and late-time behavior without the presence of growing modes.

It is worth emphasizing that, when the horizon coincides with the minimum of the areal function—which occurs for $c = 2/(3\pi A^2)$ —Eqs. (A1) and (A2) yield in the eikonal limit

$$\omega = \frac{1}{A} \sqrt{\frac{2}{\pi} \arctan\left(\frac{2}{\pi}\right) \left(\ell + \frac{1}{2} - i\left(n + \frac{1}{2}\right)\right)} + \mathcal{O}(1/\ell), \quad (67)$$

in exact agreement with the asymptotic expression reported in Ref. [24] for axial gravitational perturbations in this case.

This agreement reflects a more general property of the eikonal regime ($\ell \gg 1$), where the effective potentials

governing different types of perturbations share a universal leading-order form. In this limit, the quasinormal spectrum is determined by the properties of unstable null geodesics of the background spacetime, and therefore depends primarily on the geometry rather than on the spin of the perturbing field [62]. This explains why the scalar field QNFs obtained here coincide with those of gravitational perturbations in the same regime.

V. GREYBODY FACTORS

For frequencies satisfying $\omega^2 \approx V_0$, we make use of the WKB approximation beyond the eikonal limit. In particular, we employ the first-order WKB formula developed by Schutz and Will (see Ref. [36]) for black-hole scattering, which yields

$$R = \left(1 + e^{-2i\pi(\nu + \frac{1}{2})}\right)^{-1/2}, \quad \omega^2 \simeq V_0, \quad (68)$$

and

$$|T(\omega)|^2 = 1 - |R(\omega)|^2, \quad (69)$$

where $T(\omega)$ denotes the transmission coefficient. The quantity ν satisfies

$$\nu + \frac{1}{2} = i \frac{\omega^2 - V_0}{\sqrt{-2V_0''}} + \Lambda_2 + \Lambda_3. \quad (70)$$

Here, V_0'' denotes the second derivative of the effective potential evaluated at its maximum, while Λ_2 and Λ_3 correspond to the second- and third-order WKB corrections. These corrections depend on derivatives of the effective potential up to sixth order, all evaluated at the location of the potential peak.

The second- and third-order WKB corrections, Λ_2 and Λ_3 , take the standard form

$$\Lambda_2 = \frac{1}{(2Q_0'')^{1/2}} \left[\frac{1}{8} \left(\frac{Q_0^{(4)}}{Q_0''}\right) \left(\frac{1}{4} + N^2\right) - \frac{1}{288} \left(\frac{Q_0^{(3)}}{Q_0''}\right)^2 (7 + 60N^2) \right], \quad (71)$$

$$\Lambda_3 = \frac{N}{2Q_0''} \left[\frac{5}{6912} \left(\frac{Q_0^{(3)}}{Q_0''}\right)^4 (77 + 188N^2) - \frac{1}{384} \left(\frac{(Q_0^{(3)})^2 Q_0^{(4)}}{Q_0''^3}\right) (51 + 100N^2) \right. \\ \left. + \frac{1}{2304} \left(\frac{Q_0^{(4)}}{Q_0''}\right)^2 (67 + 68N^2) + \frac{1}{288} \left(\frac{Q_0^{(3)} Q_0^{(5)}}{Q_0''^2}\right) (19 + 28N^2) - \frac{1}{288} \left(\frac{Q_0^{(6)}}{Q_0''}\right) (5 + 4N^2) \right], \quad (72)$$

where

$$N = \nu + \frac{1}{2}, \quad Q_0^{(n)} = \left. \frac{d^n Q}{dr_*^n} \right|_{r_* = r_*(r_{\max})}, \quad Q \equiv \omega^2 - V. \quad (73)$$

The above expressions constitute the standard second-

and third-order contributions in the WKB expansion. The full method was extended up to sixth order in Ref. [54], and has since been applied extensively to scattering problems around black holes (see, for instance, Ref. [63] and references therein).

The absorption cross section is given by

$$\sigma = \sum_{\ell=0}^{\infty} \sigma_{\ell}, \quad (74)$$

where each partial contribution is computed from the transmission coefficient through

$$\sigma_{\ell} = \frac{\pi}{\omega^2} (2\ell + 1) |T(\omega)|^2. \quad (75)$$

The WKB approximation has been extensively employed to evaluate the reflection and transmission coefficients, $R(\omega)$ and $T(\omega)$, and consequently the greybody factors in a wide variety of black-hole backgrounds.

The low-frequency regime cannot be accurately described by the WKB approximation, since the method requires the wavelength of the perturbation to be much smaller than the characteristic scale of variation of the potential barrier. When $\omega^2 \ll V_0$ this condition is violated, and one must instead rely on the standard low-energy approximation, in which the transmission amplitude is exponentially suppressed. In this regime, the transmission coefficient is given by the well-known expression

$$T = e^{-\int_{z_1}^{z_2} dz \sqrt{V(z) - \omega^2}}, \quad (76)$$

where z_1 and z_2 are the classical turning points defined by $V(z) = \omega^2$. The reflection coefficient then follows as

$$R = \sqrt{1 - e^{-2 \int_{z_1}^{z_2} dz \sqrt{V(z) - \omega^2}}}. \quad (77)$$

We emphasize that the low-frequency tunneling approximation, Eqs. (71)–(72), is applicable only when the effective potential develops a genuine barrier, i.e. when two classical turning points exist. In the present model, for sufficiently small frequencies the equation $V(r) = \omega^2$ admits only a single root outside the horizon, and therefore no classically forbidden region is formed. In this regime the tunneling description is not applicable and the reflection coefficient trivially approaches unity. The low-energy formulas are thus evaluated only in the frequency interval where two turning points are present. So, at very small frequencies the reflection coefficient approaches unity, meaning that nearly all the incoming flux is reflected by the potential barrier. As the frequency increases, the transmission grows gradually, and for values of ω comparable to or larger than the height of the barrier the reflection coefficient becomes negligible.

Figure 7 displays the frequency dependence of the reflection coefficient $|R(\omega)|^2$ (top panel), the transmission coefficient $|T(\omega)|^2$ (middle panel), and the partial greybody factor $\sigma_{\ell}(\omega)$ (bottom panel), computed within the

WKB approximation for different values of the parameter A , with $c = 1$ and $\ell = 1$. Increasing A shifts the event horizon toward smaller radii and smooths the near-origin region, leading to systematic modifications of the effective potential shown in Fig. 2. Although Fig. 2 is presented for a massive probe, its qualitative structure captures the essential features governing wave scattering. In particular, increasing A the effective potential barrier becomes lower and narrower, thereby enhancing wave transmission at lower frequencies. This behavior is clearly reflected in Fig. 7, where the transition from almost complete reflection at low frequencies to dominant transmission occurs at progressively smaller values of ω as A increases. Correspondingly, the greybody factor exhibits a pronounced peak at intermediate frequencies, whose position shifts toward lower ω and whose magnitude is enhanced, signaling a more efficient absorption process.

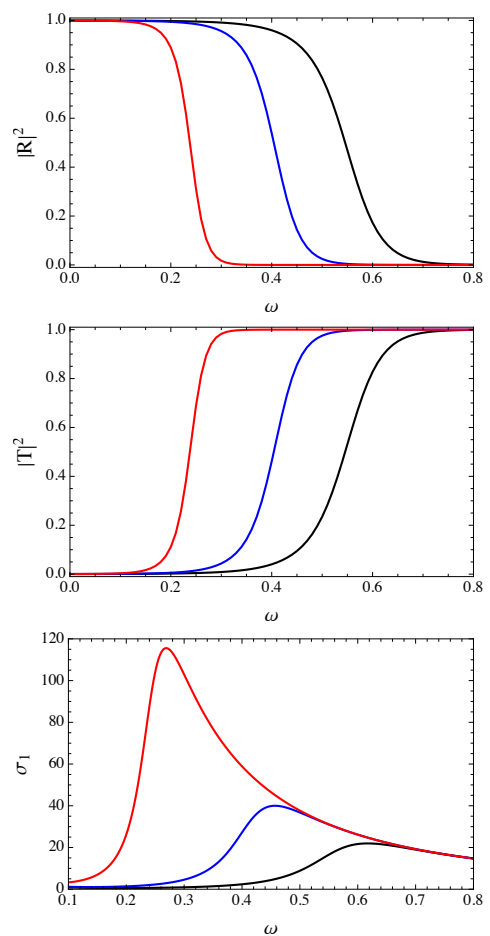


FIG. 7: Frequency dependence of the reflection coefficient $|R(\omega)|^2$ (top), the transmission coefficient $|T(\omega)|^2$ (middle), and the partial greybody factor $\sigma_{\ell}(\omega)$ (bottom), with $c = 1$. The different curves correspond to distinct values of the parameter A , $A = 0.9$ (black curve), $A = 1.0$ (blue curve), and $A = 1.2$ (red curve) while the angular momentum number ℓ is kept fixed ($\ell = 1$).

VI. CONCLUSIONS

In this work, we have investigated the dynamical response of asymptotically flat regular black holes supported by a phantom scalar field, focusing on scalar perturbations, quasinormal modes, and greybody factors. The regularizing scalar charge A smooths out the central singularity while continuously deforming the Schwarzschild geometry, allowing us to assess how regularity effects manifest themselves in wave dynamics and scattering processes.

By analyzing the effective potential governing massive scalar perturbations, we have shown that increasing the scalar charge systematically lowers and broadens the potential barrier, shifting its maximum outward while preserving asymptotic flatness. These modifications have a direct impact on the quasinormal spectrum. Using WKB techniques beyond the eikonal limit, we have demonstrated that the presence of scalar hair reduces the oscillation frequencies and increases the damping times of the modes, in agreement with the weakened confinement induced by the regular geometry. Furthermore, we have employed the Horowitz–Hubeny method and have shown that the results obtained from the WKB and Horowitz–Hubeny approaches exhibit excellent agreement in the regime where both methods are valid.

A central result of this work is the confirmation of an anomalous decay rate for massive scalar perturbations in this class of regular black holes. We have identified a critical value of the scalar field mass above which the hierarchy of damping times is inverted, so that modes with lower angular momentum become longer lived than those with higher multipole number. We derived analytical expressions for the critical mass and analyzed its dependence on the scalar charge and overtone number, and revealing how regularity effects shift the onset of the anomalous regime.

In addition, we have studied black-hole scattering by computing reflection and transmission coefficients and the associated greybody factors using WKB methods. Our analysis shows that the scalar charge leaves a clear imprint on the transmission probabilities, modifying both the height and width of the absorption window and thus affecting the frequency dependence of the greybody spectrum. These results provide a complementary characterization of regular black holes, linking quasinormal ringing and scattering properties within a unified wave-dynamical framework.

Overall, our findings indicate that regular black holes with scalar hair exhibit distinctive signatures in both their quasinormal mode spectrum and greybody factors. This reinforces the idea that wave dynamics offers a powerful probe of black-hole regularization mechanisms and scalar hair. Extensions of this work could include the analysis of other types of perturbations, different asymptotics, or the incorporation of observational constraints to further assess the phenomenological viability of regu-

lar black-hole models.

Appendix A: Full third-order WKB expressions for the QNFs and critical mass

In this appendix, we provide the complete analytical expressions for the quasinormal frequencies and the critical mass, derived using the WKB approximation at third order beyond the eikonal limit.

$$\omega_{1m} = \frac{1}{A} \sqrt{\frac{\eta}{2}}, \quad (\text{A1})$$

$$\omega_0 = -\frac{i(1+2n)\sqrt{\eta}}{2\sqrt{2}A}, \quad (\text{A2})$$

$$\begin{aligned} \omega_1 = & \frac{1}{16A} \sqrt{\frac{\eta}{2}} \left[3\pi A^6 c^3 (30n(n+1) - 61) \right. \\ & - 2A^4 c^2 (30n(n+1) - 61) \\ & + 3\pi A^2 c (2n(n+1) - 3) + 8\bar{m}^2 (9A^6 c^2 + A^2) \\ & - 6A^2 c (A^4 c^2 (30n(n+1) - 61) + 2n(n+1) - 3) \\ & \left. \times \arctan(3A^2 c) - 4(n^2 + n - 1) \right], \quad (\text{A3}) \end{aligned}$$

$$\begin{aligned} \omega_2 = & \frac{i(1+2n)}{128\sqrt{2}A} \eta^{3/2} \left[45\pi A^{10} c^5 \tilde{n} - 30A^8 c^4 \tilde{n} + 6\pi A^6 c^3 \tilde{n} \right. \\ & - 188A^4 c^2 (n^2 + n - 6) + 3\pi A^2 c (n^2 + n - 15) + \\ & \bar{m}^2 (6480A^{10} c^4 + 864A^6 c^2 + 16A^2) - 6A^2 c (15A^8 c^4 \tilde{n} \\ & + 2A^4 c^2 \tilde{n} + n^2 + n - 15) \\ & \left. \times \arctan(3A^2 c) - 2(n^2 + n + 3) \right], \quad (\text{A4}) \end{aligned}$$

where $\eta = 2 - 3\pi c A^2 + 6c A^2 \arctan(3c A^2)$, and $\tilde{n} = 47n(n+1) - 401$.

The critical mass \bar{m}_c is determined by the condition $\omega_2 = 0$, and is given by

$$\begin{aligned} \bar{m}_c = & \frac{1}{4A\sqrt{1+54c^2A^4+405c^4A^8}} \left[2(15A^8 c^4 \tilde{n} \right. \\ & + 94A^4 c^2 (n^2 + n - 6) + n^2 + n + 3) - \\ & 3\pi A^2 c (15A^8 c^4 \tilde{n} + 2A^4 c^2 \tilde{n} \\ & + n^2 + n - 15) + 6A^2 c (15A^8 c^4 \tilde{n} + \\ & \left. 2A^4 c^2 \tilde{n} + n^2 + n - 15) \tan^{-1}(3A^2 c) \right]^{1/2} \quad (\text{A5}) \end{aligned}$$

Appendix B: Near-horizon series expansions

In this appendix, we list the series expansions of the functions $s(x)$, $t(x)$ and $u(x)$ around the event horizon x_+ , which are required for the implementation of the Horowitz–Hubeny method

$$s(x) = \sum_{n=0}^5 s_n (x - x_+)^n, \quad t(x) = \sum_{n=0}^5 t_n (x - x_+)^n,$$

$$u(x) = \sum_{n=0}^5 u_n (x - x_+)^n.$$

The expansion coefficients are given by

$$s_0 = 4x_+^2 (A^2 x_+^2 + 1) \beta^2,$$

$$s_1 = 4x_+ (5A^2 x_+^2 + 3) \beta^2,$$

$$s_2 = 4 (10A^2 x_+^2 + 3) \beta^2,$$

$$s_3 = \frac{4}{x_+} (10A^2 x_+^2 + 1) \beta^2,$$

$$s_4 = 20A^2 \beta^2,$$

$$s_5 = \frac{4}{x_+} A^2 \beta^2,$$

$$t_0 = 4x_+ (A^2 x_+^2 + 1) (x_+ - 2i\omega) \beta^2,$$

$$t_1 = 4\omega^2 \left[x_+ \left(3 + A^2 x_+ \left(7x_+ - 2i(2\beta + 5\omega) \right) \right) \right. \\ \left. - 2i(2\beta + 3\omega) \right] + 4i\bar{m}^2 \left[3(\beta + 2\omega) \right. \\ \left. + x_+ \left(A^2 x_+ (3\beta + 7ix_+ + 10\omega) + 3i \right) \right],$$

$$t_2 = \frac{4\omega^2}{x_+} \left[x_+ \left(3 + 2A^2 x_+ \left(9x_+ - i(7\beta + 10\omega) \right) \right) \right. \\ \left. - 6i(\beta + \omega) \right] + \frac{4i\bar{m}^2}{x_+} \left[x_+ \left(2A^2 x_+ \left(5 \right. \right. \right. \\ \left. \left. \times (\beta + 2\omega) + 9ix_+ \right) + 3i \right) + 4\beta + 6\omega \right],$$

$$t_3 = \frac{4\omega^2}{x_+^2} \left[2A^2 x_+^2 (11x_+ - i(9\beta + 10\omega)) \right. \\ \left. - 2i(\beta + \omega) + x_+ \right] + \frac{4i\bar{m}^2}{x_+^2} \left[x_+ \left(2A^2 x_+ \right. \right. \\ \left. \left. \times (6\beta + 11ix_+ + 10\omega) + i \right) + \beta + 2\omega \right],$$

$$t_4 = \frac{4A^2}{x_+} \left[\omega^2 (13x_+ - 10i(\beta + \omega)) \right. \\ \left. + i\bar{m}^2 (6\beta + 13ix_+ + 10\omega) \right],$$

$$t_5 = \frac{4A^2}{x_+^2} \left[\omega^2 (3x_+ - 2i(\beta + \omega)) \right. \\ \left. + i\bar{m}^2 (\beta + 3ix_+ + 2\omega) \right],$$

$$\begin{aligned}
u_0 &= 0, \\
u_1 &= \frac{2\bar{m}^2}{x_+} \left[2\omega(3\beta + 5\omega) + x_+ \left(x_+ \left(iA^2 x_+ \right. \right. \right. \\
&\quad \times (3\beta + 4\omega) + 2A^2\omega(3\beta + 5\omega) \\
&\quad \left. \left. \left. - 2\ell(\ell + 1) \right) + 3i\beta \right) \right] - \frac{4\omega^2}{x_+} \left[4\omega(\beta + \omega) \right. \\
&\quad \left. + x_+ \left(x_+ \left(2iA^2 x_+ (\beta + \omega) + \right. \right. \right. \\
&\quad \left. \left. \left. 4A^2\omega(\beta + \omega) - \ell(\ell + 1) \right) + 2i\beta \right) \right] \\
&\quad - \frac{4\bar{m}^4}{x_+} (A^2 x_+^2 + 1), \\
u_2 &= \frac{2x_+ \bar{m}^2}{x_+^3} \left[-2x_+^2 \left(-A^2\omega(10\beta + 17\omega) + \ell^2 + \ell \right) \right. \\
&\quad \left. + iA^2 x_+^3 (11\beta + 16\omega) - ix_+ \beta + \right. \\
&\quad \left. 2\omega(4\beta + 7\omega) \right] - \frac{4\omega^2}{x_+^3} \left[2(\beta + \omega) \right. \\
&\quad \left. \times (7A^2 x_+^3 \omega + 4iA^2 x_+^4 + 3x_+ \omega) - \ell^2 x_+^3 - \ell x_+^3 \right] \\
&\quad - \frac{x_+ \bar{m}^4}{x_+^3} (13A^2 x_+^2 + 5), \\
u_3 &= \frac{\bar{m}^2}{x_+^3} \left[4\omega(\beta + 2\omega) + 6A^2 x_+^2 \left(2\omega(4\beta + 7\omega) \right. \right. \\
&\quad \left. \left. + ix_+ (5\beta + 8\omega) \right) \right] - \frac{8\omega^2}{x_+^3} (\beta + \omega) \\
&\quad \left(\omega + 3A^2 x_+^2 (3\omega + 2ix_+) \right) - \frac{\bar{m}^4}{x_+^3} (15A^2 x_+^2 + 1), \\
u_4 &= \frac{2\bar{m}^2 A^2}{x_+^2} \left[2\omega(6\beta + 11\omega) + ix_+ (9\beta \right. \\
&\quad \left. + 16\omega) \right] - \frac{8\omega^2 A^2}{x_+^2} (5\omega + 4ix_+) (\beta + \omega) - \frac{7\bar{m}^4 A^2}{x_+^2}, \\
u_5 &= \frac{4\bar{m}^2 A^2}{x_+^3} (\omega + ix_+) (\beta + 2\omega) - \frac{8\omega^2 A^2}{x_+^3} (\omega + ix_+) \\
&\quad \times (\beta + \omega) - \frac{\bar{m}^4 A^2}{x_+^3},
\end{aligned}$$

where $\beta^2 = \omega^2 - \bar{m}^2$.

Acknowledgments

We thank the anonymous referee for valuable comments and suggestions. Y. V. acknowledges support by

the Dirección de Investigación y Desarrollo de la Universidad de La Serena, Grant No. PR25538511.

-
- [1] B. Wang, E. Abdalla, F. Atrio-Barandela, D. Pavón “Dark Matter and Dark Energy Interactions: Theoretical Challenges, Cosmological Implications and Observational Signatures,” *Rept.Prog.Phys.* **79** (2016) 9, 096901.
- [2] A. Upadhye, M. Ishak and P. J. Steinhardt, “Dynamical dark energy: Current constraints and forecasts,” *Phys. Rev. D* **72** (2005), 063501 [arXiv:astro-ph/0411803 [astro-ph]].
- [3] Y. Wang and M. Tegmark, “New dark energy constraints from supernovae, microwave background and galaxy clustering,” *Phys. Rev. Lett.* **92** (2004), 241302 [arXiv:astro-ph/0403292 [astro-ph]].
- [4] U. Seljak *et al.* [SDSS], “Cosmological parameter analysis including SDSS Ly-alpha forest and galaxy bias: Constraints on the primordial spectrum of fluctuations, neutrino mass, and dark energy,” *Phys. Rev. D* **71** (2005), 103515 [arXiv:astro-ph/0407372 [astro-ph]].
- [5] S. Hannestad and E. Mortsell, “Cosmological constraints on the dark energy equation of state and its evolution,” *JCAP* **09** (2004), 001 [arXiv:astro-ph/0407259 [astro-ph]].
- [6] U. Alam, V. Sahni, T. D. Saini and A. A. Starobinsky, “Is there supernova evidence for dark energy metamorphosis?,” *Mon. Not. Roy. Astron. Soc.* **354** (2004), 275 [arXiv:astro-ph/0311364 [astro-ph]].
- [7] S. W. Allen, R. W. Schmidt, H. Ebeling, A. C. Fabian and L. van Speybroeck, “Constraints on dark energy from Chandra observations of the largest relaxed galaxy clusters,” *Mon. Not. Roy. Astron. Soc.* **353** (2004), 457 [arXiv:astro-ph/0405340 [astro-ph]].
- [8] A. Sen, “Rolling tachyon,” *JHEP* **04** (2002), 048 [arXiv:hep-th/0203211 [hep-th]]. “Tachyon matter,” *JHEP* **07** (2002), 065 [arXiv:hep-th/0203265 [hep-th]].
- [9] V. Gorini, A. Y. Kamenshchik, U. Moschella and V. Pasquier, “Tachyons, scalar fields and cosmology,” *Phys. Rev. D* **69** (2004), 123512 [arXiv:hep-th/0311111 [hep-th]].
- [10] V. Faraoni, “Phantom cosmology with general potentials,” *Class. Quant. Grav.* **22** (2005), 3235-3246 [arXiv:gr-qc/0506095 [gr-qc]].
- [11] S. Nojiri and S. D. Odintsov, “Quantum de Sitter cosmology and phantom matter,” *Phys. Lett. B* **562** (2003), 147-152 [arXiv:hep-th/0303117 [hep-th]].
- [12] S. M. Carroll, M. Hoffman and M. Trodden, “Can the dark energy equation-of-state parameter w be less than -1 ?,” *Phys. Rev. D* **68** (2003), 023509, [arXiv:astro-ph/0301273 [astro-ph]].
- [13] J. Bardeen, In: *Proceedings of GR5, Tiflis, USSR* (1968).
- [14] D. Farrah, K. S. Croker, G. Tarlé, V. Faraoni, S. Petty, J. Afonso, N. Fernandez, K. A. Nishimura, C. Pearson and L. Wang, *et al.* “Observational Evidence for Cosmological Coupling of Black Holes and its Implications for an Astrophysical Source of Dark Energy,” *Astrophys. J. Lett.* **944**, no.2, L31 (2023) [arXiv:2302.07878 [astro-ph.CO]].
- [15] Akiyama, K., Alberdi, A., Alef, W., et al. 2022, *The Astrophysical Journal Letters*, 930, L12.
- [16] K. A. Bronnikov and J. C. Fabris, “Regular phantom black holes,” *Phys. Rev. Lett.* **96** (2006), 251101 [arXiv:gr-qc/0511109 [gr-qc]]. K. A. Bronnikov, “Scalar fields as sources for wormholes and regular black holes,” *Particles* **1** (2018) no.1, 56-81 [arXiv:1802.00098 [gr-qc]].
- [17] I. Dymnikova, “Vacuum nonsingular black hole,” *Gen. Rel. Grav.* **24**, 235-242 (1992).
- [18] K. A. Bronnikov, “Regular magnetic black holes and monopoles from nonlinear electrodynamics,” *Phys. Rev. D* **63** (2001), 044005. [arXiv:gr-qc/0006014 [gr-qc]].
- [19] K. A. Bronnikov, A. Dobosz and I. G. Dymnikova, “Nonsingular vacuum cosmologies with a variable cosmological term,” *Class. Quant. Grav.* **20** (2003), 3797-3814 [arXiv:gr-qc/0302029 [gr-qc]].
- [20] T. Karakasis, N. E. Mavromatos and E. Papantonopoulos, “Regular compact objects with scalar hair,” *Phys. Rev. D* **108**, no.2, 024001 (2023) [arXiv:2305.00058 [gr-qc]].
- [21] K. D. Kokkotas and B. G. Schmidt, “Quasinormal modes of stars and black holes,” *Living Rev. Rel.* **2**, 2 (1999) [arXiv:gr-qc/9909058 [gr-qc]].
- [22] E. Berti, V. Cardoso and A. O. Starinets, “Quasinormal modes of black holes and black branes,” *Class. Quant. Grav.* **26**, 163001 (2009) [arXiv:0905.2975 [gr-qc]].
- [23] R. A. Konoplya and A. Zhidenko, “Quasinormal modes of black holes: From astrophysics to string theory,” *Rev. Mod. Phys.* **83**, 793-836 (2011) [arXiv:1102.4014 [gr-qc]].
- [24] K. A. Bronnikov, R. A. Konoplya and A. Zhidenko, “Instabilities of wormholes and regular black holes supported by a phantom scalar field,” *Phys. Rev. D* **86** (2012), 024028 [arXiv:1205.2224 [gr-qc]].
- [25] O. Dreyer, B. J. Kelly, B. Krishnan, L. S. Finn, D. Garrison and R. Lopez-Aleman, “Black hole spectroscopy: Testing general relativity through gravitational wave observations,” *Class. Quant. Grav.* **21** (2004), 787-804 [arXiv:gr-qc/0309007 [gr-qc]].
- [26] E. Berti, V. Cardoso and C. M. Will, “On gravitational-wave spectroscopy of massive black holes with the space interferometer LISA,” *Phys. Rev. D* **73** (2006), 064030 [arXiv:gr-qc/0512160 [gr-qc]].
- [27] V. Cardoso, E. Franzin and P. Pani, “Is the gravitational-wave ringdown a probe of the event horizon?,” *Phys. Rev. Lett.* **116** (2016) no.17, 171101 [erratum: *Phys. Rev. Lett.* **117** (2016) no.8, 089902] [arXiv:1602.07309 [gr-qc]].
- [28] M. Isi, M. Giesler, W. M. Farr, M. A. Scheel and S. A. Teukolsky, “Testing the no-hair theorem with GW150914,” *Phys. Rev. Lett.* **123** (2019) no.11, 111102 [arXiv:1905.00869 [gr-qc]].
- [29] A. Buonanno and T. Damour, “Transition from inspiral to plunge in binary black hole coalescences,” *Phys. Rev. D* **62** (2000), 064015 [arXiv:gr-qc/0001013 [gr-qc]].
- [30] P. Ajith, S. Babak, Y. Chen, M. Hewitson, B. Krishnan, A. M. Sintes, J. T. Whelan, B. Bruegmann, P. Diener and

- N. Dorband, *et al.* “A Template bank for gravitational waveforms from coalescing binary black holes. I. Non-spinning binaries,” *Phys. Rev. D* **77** (2008), 104017 [erratum: *Phys. Rev. D* **79** (2009), 129901] [arXiv:0710.2335 [gr-qc]].
- [31] S. Husa, S. Khan, M. Hannam, M. Pürrer, F. Ohme, X. Jiménez Forteza and A. Bohé, “Frequency-domain gravitational waves from nonprecessing black-hole binaries. I. New numerical waveforms and anatomy of the signal,” *Phys. Rev. D* **93** (2016) no.4, 044006 [arXiv:1508.07250 [gr-qc]].
- [32] S. Khan, S. Husa, M. Hannam, F. Ohme, M. Pürrer, X. Jiménez Forteza and A. Bohé, “Frequency-domain gravitational waves from nonprecessing black-hole binaries. II. A phenomenological model for the advanced detector era,” *Phys. Rev. D* **93** (2016) no.4, 044007 [arXiv:1508.07253 [gr-qc]].
- [33] A. Aragón, P. A. González, E. Papantonopoulos and Y. Vásquez, “Anomalous decay rate of quasinormal modes in Schwarzschild-dS and Schwarzschild-AdS black holes,” *JHEP* **08** (2020), 120 [arXiv:2004.09386 [gr-qc]].
- [34] A. Aragón, P. A. González, E. Papantonopoulos and Y. Vásquez, “Quasinormal modes and their anomalous behavior for black holes in $f(R)$ gravity,” *Eur. Phys. J. C* **81** (2021) no.5, 407 [arXiv:2005.11179 [gr-qc]].
- [35] R. D. B. Fontana, P. A. González, E. Papantonopoulos and Y. Vásquez, “Anomalous decay rate of quasinormal modes in Reissner-Nordström black holes,” *Phys. Rev. D* **103** (2021) no.6, 064005 [arXiv:2011.10620 [gr-qc]].
- [36] R. Bécar, P. A. González, F. Moncada and Y. Vásquez, “Massive scalar field perturbations in Weyl black holes,” *Eur. Phys. J. C* **83**, no.10, 942 (2023) [arXiv:2304.00663 [gr-qc]].
- [37] R. A. Konoplya and A. Zhidenko, “Stability and quasinormal modes of the massive scalar field around Kerr black holes,” *Phys. Rev. D* **73** (2006), 124040 [arXiv:gr-qc/0605013 [gr-qc]].
- [38] S. R. Dolan, “Instability of the massive Klein-Gordon field on the Kerr spacetime,” *Phys. Rev. D* **76** (2007), 084001 [arXiv:0705.2880 [gr-qc]].
- [39] M. Lagos, P. G. Ferreira and O. J. Tattersall, “Anomalous decay rate of quasinormal modes,” *Phys. Rev. D* **101** (2020) no.8, 084018 [arXiv:2002.01897 [gr-qc]].
- [40] R. Bécar, P. A. González, E. Papantonopoulos and Y. Vásquez, “Massive scalar field perturbations of black holes surrounded by dark matter,” *Eur. Phys. J. C* **84** (2024) no.3, 329 [arXiv:2310.00857 [gr-qc]].
- [41] R. Bécar, P. A. González, E. Papantonopoulos and Y. Vásquez, “Massive scalar field perturbations of black holes immersed in Chaplygin-like dark fluid,” *JCAP* **06**, 061 (2024) [arXiv:2403.11306 [gr-qc]].
- [42] R. Bécar, P. A. González, E. Papantonopoulos and Y. Vásquez, “Massive scalar field perturbations of 4D de Sitter–Einstein–Gauss–Bonnet black holes,” *Phys. Rev. D* **111**, no.12, 124013 (2025) [arXiv:2505.17161 [gr-qc]].
- [43] G. Kouniatis, P. A. González, E. Papantonopoulos and Y. Vásquez, “Near-horizon geodesic instabilities and anomalous decay of quasinormal modes in Weyl black holes,” *Phys. Rev. D* **112**, no.12, 124061 (2025) [arXiv:2509.05164 [gr-qc]].
- [44] P. A. González, E. Papantonopoulos, J. Saavedra and Y. Vásquez, “Quasinormal modes for massive charged scalar fields in Reissner-Nordström dS black holes: anomalous decay rate,” *JHEP* **06** (2022), 150 [arXiv:2204.01570 [gr-qc]].
- [45] R. Bécar, P. A. González and Y. Vásquez, “Quasinormal modes of a charged scalar field in Ernst black holes,” *Eur. Phys. J. C* **83**, no.1, 75 (2023) [arXiv:2211.02931 [gr-qc]].
- [46] A. Aragón, R. Bécar, P. A. González and Y. Vásquez, “Massive Dirac quasinormal modes in Schwarzschild–de Sitter black holes: Anomalous decay rate and fine structure,” *Phys. Rev. D* **103**, no.6, 064006 (2021) [arXiv:2009.09436 [gr-qc]].
- [47] K. Destounis, R. D. B. Fontana and F. C. Mena, “Accelerating black holes: quasinormal modes and late-time tails,” *Phys. Rev. D* **102**, no.4, 044005 (2020) [arXiv:2005.03028 [gr-qc]].
- [48] P. A. González, E. Papantonopoulos, Á. Rincón and Y. Vásquez, “Quasinormal modes of massive scalar fields in four-dimensional wormholes: Anomalous decay rate,” *Phys. Rev. D* **106** (2022) no.2, 024050 [arXiv:2205.06079 [gr-qc]].
- [49] S. Alfaro, P. A. González, D. Olmos, E. Papantonopoulos and Y. Vásquez, “Quasinormal modes and bound states of massive scalar fields in wormhole spacetimes,” *Phys. Rev. D* **109** (2024) no.10, 104009 [arXiv:2402.15575 [gr-qc]].
- [50] P. A. González, M. Olivares, E. Papantonopoulos and Y. Vásquez, “Observational Tests of Regular Black Holes with Scalar Hair and their Stability,” [arXiv:2510.18647 [gr-qc]].
- [51] D. C. Zou and Y. S. Myung, “Black hole with primary scalar hair in Einstein–Weyl–Maxwell–conformal scalar theory,” *Phys. Rev. D* **101**, no.8, 084021 (2020) [arXiv:2001.01351 [gr-qc]]; A. Anabalon, F. Canfora, A. Giacomini and J. Oliva, “Black Holes with Primary Hair in gauged $N=8$ Supergravity,” *JHEP* **06**, 010 (2012) [arXiv:1203.6627 [hep-th]]; S. Mignemi and D. L. Wiltshire, “Multi-scalar black holes with contingent primary hair: Mechanics and stability,” *Phys. Rev. D* **70**, 124012 (2004) [arXiv:hep-th/0408215 [hep-th]]; S. Mignemi, “Primary scalar hair in dilatonic theories with modulus fields,” *Phys. Rev. D* **62**, 024014 (2000) [arXiv:gr-qc/9910041 [gr-qc]]; P. A. González, E. Papantonopoulos, J. Saavedra and Y. Vásquez, “Four-Dimensional Asymptotically AdS Black Holes with Scalar Hair,” *JHEP* **12** (2013), 021 [arXiv:1309.2161 [gr-qc]].
- [52] B. Mashhoon, “Quasi-normal modes of a black hole,” Third Marcel Grossmann Meeting on General Relativity 1983.
- [53] B. F. Schutz and C. M. Will, “Black hole normal modes: a semianalytic approach,” *Astrophys. J. Lett.* **291** (1985), L33–L36.
- [54] S. Iyer and C. M. Will, “Black Hole Normal Modes: A WKB Approach. 1. Foundations and Application of a Higher Order WKB Analysis of Potential Barrier Scattering,” *Phys. Rev. D* **35** (1987), 3621.
- [55] R. A. Konoplya, “Quasinormal behavior of the d-dimensional Schwarzschild black hole and higher order WKB approach,” *Phys. Rev. D* **68** (2003), 024018 [arXiv:gr-qc/0303052 [gr-qc]].
- [56] J. Matyjasek and M. Opala, “Quasinormal modes of black holes. The improved semianalytic approach,” *Phys. Rev. D* **96** (2017) no.2, 024011 [arXiv:1704.00361 [gr-qc]].
- [57] R. A. Konoplya, A. Zhidenko and A. F. Zinhailo, “Higher order WKB formula for quasinormal modes

- and grey-body factors: recipes for quick and accurate calculations,” *Class. Quant. Grav.* **36** (2019), 155002 [arXiv:1904.10333 [gr-qc]].
- [58] Y. Hatsuda, “Quasinormal modes of black holes and Borel summation,” *Phys. Rev. D* **101**, no.2, 024008 (2020) [arXiv:1906.07232 [gr-qc]].
- [59] G. T. Horowitz and V. E. Hubeny, “Quasinormal modes of AdS black holes and the approach to thermal equilibrium,” *Phys. Rev. D* **62**, 024027 (2000) [arXiv:hep-th/9909056 [hep-th]].
- [60] Müller, David E., “A Method for Solving Algebraic Equations Using an Automatic Computer,” *MTAC*, 10 (1956), 208-215.
- [61] R. L. Burden and J. D. Faires, “Numerical Analysis,” 7th Edition, Addison-Wesley Inc., New York, 2000.
- [62] V. Cardoso, A. S. Miranda, E. Berti, H. Witek and V. T. Zanchin, “Geodesic stability, Lyapunov exponents and quasinormal modes,” *Phys. Rev. D* **79**, no.6, 064016 (2009) [arXiv:0812.1806 [hep-th]].
- [63] J. Grain and A. Barrau, *Nucl. Phys. B* 742, 253 (2006) [arXiv:hep-th/0603042]. P. Kanti and R. A. Konoplya, *Phys. Rev. D* 73, 044002 (2006) [arXiv:hep-th/0512257]; H. Kodama, R. A. Konoplya and A. Zhidenko, arXiv:0904.2154 [gr-qc]; S. K. Chakrabarti, *Eur. Phys. J. C* 61, 477 (2009) [arXiv:0809.1004 [gr-qc]]; Y. Zhang, Y. X. Gui and F. Yu, *Chin. Phys. Lett.* 26 (2009) 030401 [arXiv:0710.5064 [gr-qc]].